Rock Mechanics and Rock Engineering
https://doi.org/10.1007/s00603-026-05743-1

ORIGINAL PAPER

Mineral Strengthening and Crack Weakening Jointly Control the Physical–mechanical Properties of Shocked Planetary Rocks

Yiheng Zhang[1] · Jiangmei Qiao[1] · Haifeng Zhao[2] · Pengzhi Pan[3] · Xuhai Tang[1]

Received: 5 December 2025 / Accepted: 14 June 2026
© The Author(s), under exclusive licence to Springer-Verlag GmbH Austria, part of Springer Nature 2026

Abstract

Planetary impacts not only reshape planetary surfaces but also fundamentally alter rock properties at the nanoscale. By analyzing the Hammadah al Hamra 346 (HaH 346) chondrite containing shock melt veins, we find that shock not only causes the transformation of some minerals into high-pressure phases (wadsleyite and jadeite) but also induces grain refinement. The average crystal grain size decreases from 16.71 μm to 0.74 μm, resulting in an increase of ~ 70% in the elastic modulus and hardness of all minerals, including both high-pressure and non-high-pressure phases. At the rock scale, mechanical behavior is controlled by a competition between mineral strengthening and crack weakening. When contraction cracks are present and dominant, the mechanical strength and P-wave velocity of rocks are reduced, consistent with observations from the Charlevoix and Chesapeake Bay impact structures. In contrast, in the absence of such cracks, mineral strengthening dominates, leading to increases of 20–50% in rock mechanical strength and P-wave velocity. This study establishes a cross-scale framework that links crystal grains, mineral grains, and rocks, revealing how impact processes influence the physical–mechanical properties of planetary surfaces.

Highlights

- A crystal-mineral-rock framework is established to link shock-induced nanostructuring with physical-mechanical properties of planetary rock.
- Shock melt veins show strong grain refinement that strengthens minerals.
- Shock melt veins without contraction cracks strengthen rocks; in contrast, contraction cracks significantly weaken rocks and reduce P-wave velocity.

Keywords Planetary impacts · Physical–mechanical properties · Grain refinement · Crystal-mineral-rock framework · Meteorites

1 Introduction

Planetary defence, extraterrestrial construction, and planetary evolution studies urgently require an understanding of the physical–mechanical properties of planetary rocks. However, the fundamental physical–mechanical properties of extraterrestrial geomaterials remain poorly constrained (Witze 2021; Robin et al. 2024; Khan et al. 2021). This knowledge gap has directly led to a number of mission setbacks, for instance, the Curiosity rover's coring failure in Gale Crater (Vasavada 2022), the InSight HP^3 "Mole" probe halting after penetrating only about 30–40 cm instead of the planned 5 m (Spohn et al. 2018), and the Perseverance rover's first unsuccessful coring attempt in Jezero Crater (Witze 2021). Moreover, insufficient understanding of extraterrestrial rocks has significantly hindered the interpretation of seismic inversions (Xiao et al. 2025) and radar data (Orosei

✉ Xuhai Tang
xuhaitang@whu.edu.cn

1 School of Civil Engineering, Wuhan University, Wuhan 430072, China

2 Technology and Engineering Center for Space Utilization, Chinese Academy of Sciences, Beijing 100094, China

3 State Key Laboratory of Geomechanics and Geotechnical Engineering, Institute of Rock and Soil Mechanics, Chinese Academy of Sciences, Wuhan 430071, China

Published online: 10 July 2026

et al. 2018), thereby limiting the scientific understanding of planetary internal structures (Kronyak et al. 2020).

High velocity impact-related geological phenomena are widely distributed across the surfaces of Earth, the Moon, Mars, and asteroids. These processes not only profoundly shape planetary surface morphology but also significantly alter the physical–mechanical properties of geomaterials. Impact craters are important target areas for planetary exploration and landing missions. Martian craters such as Gale, Jezero, and Gusev (Mangold et al. 2021), as well as lunar craters including Von Kármán, Tycho, and Copernicus (Li et al. 2020; Ghent et al. 2016), have all been selected as sites for landing and exploration missions. To understand the formation mechanisms and characteristics of impact craters, researchers have conducted extensive observations of terrestrial impact structures to investigate the formation processes and impact characteristics of various events (Collins et al. 2020). However, most impact craters on Earth have undergone significant erosion or modification, making it difficult to preserve their original impact features intact (Collins et al. 2004). In contrast, shock melt veins preserved in meteorites are less affected by terrestrial weathering and retain direct records of shock metamorphism on parent asteroids, including localized melting, phase transformation, and shock-induced microstructural modification. These features provide ideal natural samples for investigating how impact processes modify the intrinsic physical and mechanical properties of planetary materials and contribute to the long-term evolution of asteroid parent bodies (Kohout et al. 2017, 2020; Bischoff et al. 2019).

The rapid advancement of microscale experimental techniques has provided a new approach for investigating the physical–mechanical properties of planetary geomaterials using meteorites. These techniques have been widely applied to characterize the mechanical properties of minerals and interphases in terrestrial rocks (Tang et al. 2022) and have been well validated in research on mineral-rock physical–mechanical properties (Xu et al. 2023). More recently, these techniques have been extended to extraterrestrial materials, including various meteorites and lunar samples, enabling systematic characterization of their microscale mechanical heterogeneity (Tang et al. 2023; Grebol-Tomas et al. 2025; Nie et al. 2025). In particular, nanoindentation studies of the Chelyabinsk meteorite demonstrate that local mechanical properties of ordinary chondrites can provide important constraints on the mechanical response of asteroid materials during impact and deflection processes (Moyano-Cambero et al. 2017a, 2017b). Moreover, nanoindentation measurements on particles returned from the surface of asteroid 25,143 Itokawa by the Hayabusa mission further demonstrate the applicability of microscale mechanical testing to sample-returned asteroid materials (Tanbakouei et al. 2019). These studies provide an important bridge between meteorite-based laboratory investigations and the physical–mechanical interpretation of chondritic asteroid materials.

This study conducts a cross-scale investigation on the Hammadah al Hamra 346 (HaH 346) L6 ordinary chondrite containing shock melt veins. We propose a crystal-mineral-rock framework, linking nanoscale grain refinement, mineral elastic modulus and hardness, and rock physical–mechanical properties with observable seismic signals, thereby establishing a new physical connection between the multiscale physical–mechanical responses of planetary rocks and their seismic characteristics.

2 Materials and Methods

2.1 HaH 346 Meteorite

As shown in Fig. 1, the HaH 346 meteorites contain abundant shock melt veins with various morphologies, including thin vein, thick vein, vein with variable widths and branching veins. HaH 346 likely fell in 2018 and is classified as a typical L6 ordinary chondrite with a weathering grade of W0. For sample preparation, we selected specimens with different shock melt veins and fresh, matte-black fusion crust to minimize the effects of terrestrial weathering.

2.2 Crystal-Mineral-Rock Methodology

We establish a cross-scale framework linking the nanomechanical properties of rock-forming minerals to the physical–mechanical properties of rocks.The following methods are used:

(1) Crystal grain-size analysis

Electron backscatter diffraction (EBSD) was used to quantify crystal grain sizes with sub-micrometre resolution, enabling a direct comparison between the host rock and shock melt veins (Bidgood et al. 2021). EBSD data were acquired using a TESCAN CLARA scanning electron microscope (SEM) equipped with an Oxford Symmetry 2 EBSD detector. The analyses were performed at an accelerating voltage of 15 kV, a beam current of 65 µA, and a step size of 0.1–0.5 µm. The EBSD patterns were processed using AZtec HKL software, and wild spikes, defined as isolated pixels with orientations different from their neighboring pixels, were removed during data cleaning. Grain boundaries were defined using a misorientation threshold of 10° between neighboring pixels within each phase. The grain size of each phase was calculated from

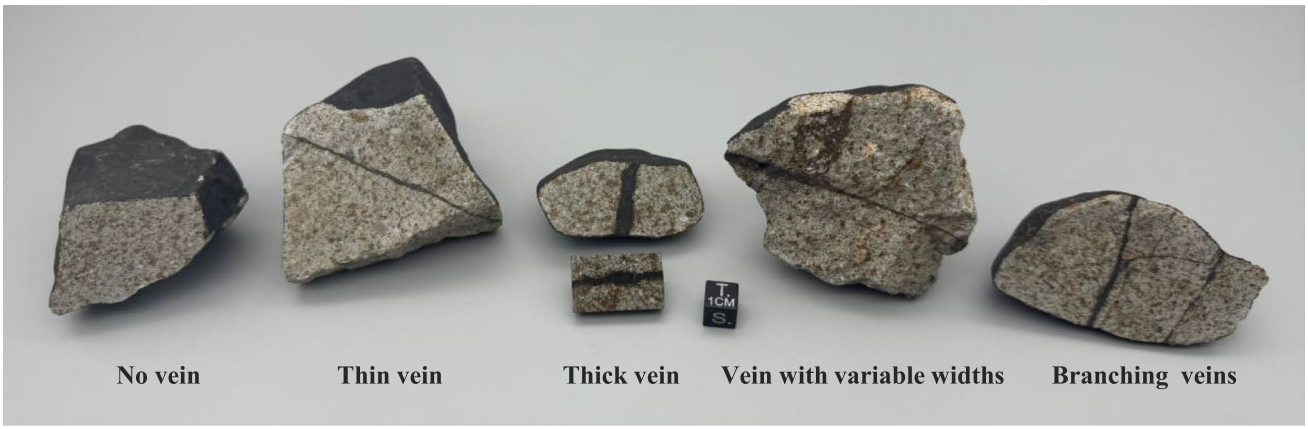

Fig. 1 HaH 346 meteorites with different shock melt veins

the equivalent circle diameter of the grains identified in the EBSD maps.

(2) Mineralogical and microstructural characterization

High-pressure mineral phases within shock melt veins were identified using scanning electron microscopy (SEM) and Raman spectroscopy, which provide complementary information on microstructural features and crystal structures (Chen et al. 2004). The mineral composition and spatial distribution of rock-forming minerals were further quantified using a TESCAN Integrated Mineral Analyzer (TIMA) (Hrstka et al. 2018). SEM observations were performed using a Zeiss SIGMA scanning electron microscope in backscattered electron (BSE) mode. BSE images were used to characterize the textures of the host rock and shock melt veins, identify mineral boundaries, and examine the spatial distribution of high-pressure phases. The SEM analyses were conducted at an accelerating voltage of 20 kV and a working distance of 6–8 mm.

Raman spectroscopy was carried out using a XploRA Plus confocal Raman microscope to identify high-pressure mineral phases within the shock melt veins. Raman spectra were collected using a 532 nm laser with a power of 5 mW, and a laser spot diameter of approximately 1 μm. The obtained spectra were compared with reference spectra from the RRUFF database (http://www.rruff.info) to confirm the presence of wadsleyite and jadeite.

Mineralogical mapping was conducted using a TESCAN Integrated Mineral Analyzer (TIMA3 X GMH). Mineral phases were identified based on a combination of BSE intensity and energy-dispersive X-ray spectroscopy (EDS) data. To efficiently characterize the relatively coarse-grained texture of the meteorite, BSE signals were acquired at a pixel spacing of 3 μm, although EDS spectra (> 1000 counts) were collected at a pixel spacing of 9 μm. The TIMA data were subsequently used to quantify the modal abundance and spatial distribution of major mineral phases, including olivine, low-Ca pyroxene, plagioclase, kamacite, and troilite.

(3) Mineral-scale mechanical testing

Mineral-scale mechanical properties were measured by nanoindentation. Tests were performed on individual mineral grains in both the host rock and shock melt veins to compare the mechanical responses of the same mineral phases before and after shock-induced modification. Nanoindentation was conducted using a Hysitron TI950 TriboIndenter system (Hysitron, Inc., Minneapolis, MN, USA) equipped with a Berkovich diamond indenter. Before testing, the indenter area function and frame compliance were calibrated using fused silica.

The maximum load was set to 4 mN, with a loading time of 5 s, a holding time of 2 s, and an unloading time of 5 s. Thermal drift correction was performed before each indentation according to the instrument procedure. For each mineral phase and textural domain, at least 50 valid indents were retained. Indents located near pores, cracks, grain boundaries, or mixed-phase regions were excluded to minimize the influence of local heterogeneity. The elastic modulus and hardness were calculated from the unloading segments of the load–displacement curves using the Oliver and Pharr (1992) method.

(4) Rock-scale mechanical and ultrasonic testing

Rock-scale mechanical properties were evaluated using uniaxial compression tests and ultrasonic P-wave velocity measurements. Cylindrical specimens with a diameter of 10 mm and a height of 20 mm were prepared from HaH 346 fragments. Both specimen ends were ground to ensure parallel loading surfaces. Uniaxial compression tests were

conducted using an Instron 5969 materials testing instrument at a stress loading rate of 50 MPa/min. Axial stress–strain curves were recorded during loading. The elastic modulus was calculated from the approximately linear elastic portion of the stress–strain curve, and the uniaxial compressive strength was determined as the peak axial stress.

Ultrasonic P-wave velocity measurements were performed to assess the effects of shock melt veins and contraction cracks on wave propagation. The measurements were conducted using a KON-NM-4A non-metallic ultrasonic testing analyzer equipped with 50 kHz P-wave transducers. A coupling agent was applied between the transducers and specimen surfaces to ensure stable acoustic transmission. The propagation direction relative to the shock melt veins and contraction cracks was recorded for each specimen (Jaeger et al. 2007). Each measurement was repeated five times, and the average value was used for analysis.

(5) Accurate grain-based modeling

Accurate grain-based models (AGBMs) with a height of 20 mm and a width of 10 mm were constructed to investigate the rock-scale mechanical effects of shock melt veins and cooling-induced contraction cracks. The model geometry was generated based on mineralogical and microstructural observations from TIMA images. Interphase elements were inserted along the boundaries of rock-forming minerals. The material parameters of mineral elements in the host rock and shock melt vein domains were assigned based on mineral-scale mechanical properties obtained from nanoindentation and atomic force microscopy tests (Tang et al. 2023).

A vertical displacement of 2 mm was applied to the upper boundary of the computational model, although the bottom boundary was constrained in the vertical direction. The loading rate was kept constant at 0.02 mm per step during the loading process. A time step of 5×10^{-4} ms was used to ensure numerical stability for the explicit time integration scheme. The simulated stress–strain curves were used to calculate the elastic modulus and uniaxial compressive strength.

3 Results

3.1 Mineralogical Contrast Between Host Rock and Shock Melt Veins

A polished section of the HaH 346 ordinary chondrite containing a distinct shock melt vein was examined by integrated mineral analysis (TIMA), SEM, and Raman spectroscopy. Both the host rock and shock melt vein comprise similar primary minerals, including olivine (38.86 vol%), low-Ca pyroxene (34.22 vol%), kamacite (11.50 vol%), plagioclase (8.17 vol%), and troilite (5.25 vol%).

High-pressure phases occur exclusively within shock melt veins, marking localized transformation under extreme shock. As shown in Fig. 2, Raman spectra reveal partial conversion of olivine to wadsleyite (Fritz and Greshake. 2009) and low-Ca pyroxene to jadeite (Miyahara et al. 2013), with EBSD estimates placing their total abundance below 1 vol%. Thus, under conventional mineral classification schemes, the shock melt vein retains both the primary mineral assemblage of a typical chondrite and trace high-pressure transformations.

3.2 Crystal Grain Size Contrast Between Host Rock and Shock Melt Veins

EBSD analyses reveal extreme grain refinement in shock melt veins (Fig. 3). Average crystal grain sizes of olivine, low-Ca pyroxene, plagioclase, troilite, and FeNi metal decrease from 21.89–7.98 μm in the host rock to ~ 0.53–0.95 μm in the shock melt veins, although newly crystallized wadsleyite and jadeite are even finer (~ 0.20–0.28 μm). Shock melting thus reduces primary crystal grains to 1/32–1/11 of their original size, with high-pressure phases refined to as little as 1/78. These results demonstrate the pervasive and intensified crystal grain size reduction of minerals under impact conditions.

3.3 Shock-Induced Elastic Modulus and Hardness Enhancement of Minerals

Then, the elastic modulus and hardness of individual rock-forming minerals were measured using nanoindentation. Nanoindentation measurements show that minerals in shock melt veins are systematically stronger than those in the host rock. Along profiles from host rock into the shock melt veins, elastic modulus rises from ~ 20–140 GPa to ~ 100–190 GPa, and hardness from ~ 1–9 GPa to ~ 4–17 GPa, reflecting strengthening associated with shock history (Fig. 4a).

As shown in Fig. 4b, c, the same mineral exhibits higher mechanical properties in the shock melt veins than in the host rock. In the host rock, olivine, low-Ca pyroxene, plagioclase, kamacite, and troilite have elastic moduli of 45.9–151.0 GPa and hardnesses of 2.48–9.44 GPa, whereas in the shock melt veins these values increase to 81.9–242.9 GPa and 2.88–12.66 GPa, respectively. The two

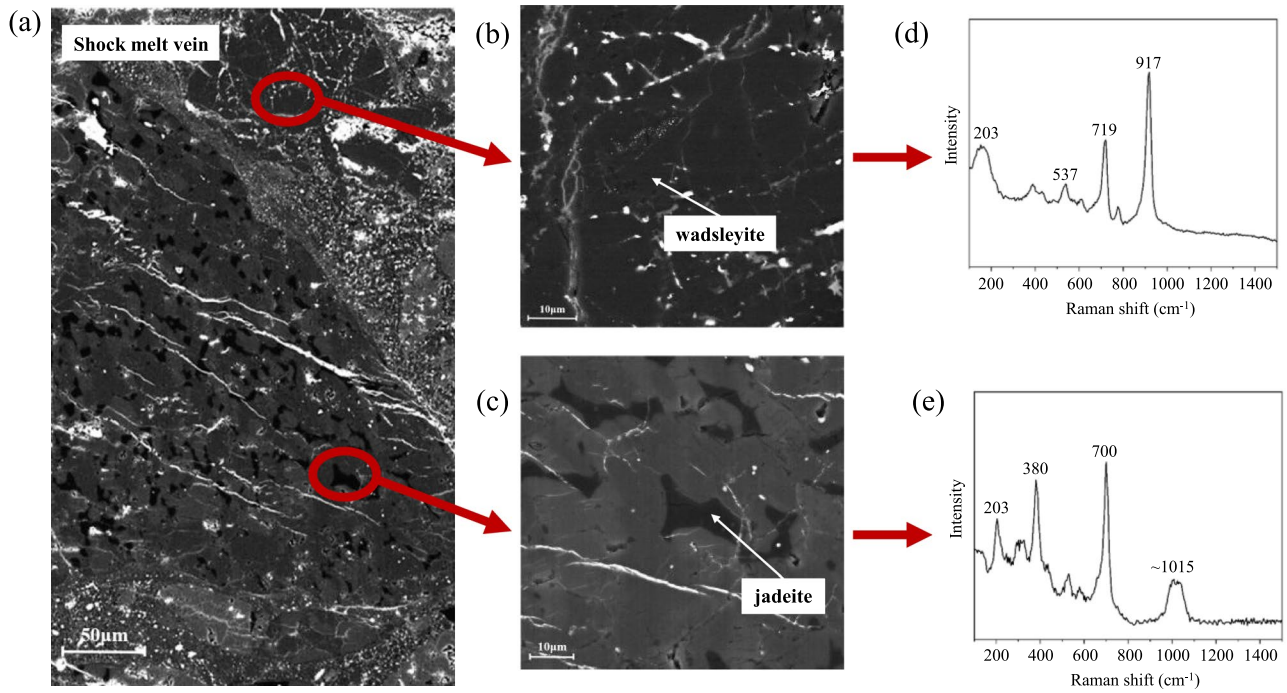

Fig. 2 High-pressure phases occur in the shock melt vein. **a** BSE images of local shock melt vein; **b**, **c** higher magnification images of wadsleyite and jadeite; **d**, **e** Raman spectra of wadsleyite and jadeite

high-pressure phases, wadsleyite and jadeite, have elastic moduli of 209.75 and 189.33 GPa, and hardnesses of 13.08 and 12.21 GPa, respectively. These results indicate systematic strengthening of minerals in the shock melt veins due to past high-velocity impacts.

3.4 Cooling-Induced Contraction Cracks in Shock Melt Veins (Observed Only in Some Samples)

Cooling-induced contraction cracks occur in some samples but are absent in others. As shown in Fig. 5, polygonal cracks within shock melt veins indicate cooling origins. CT scans of cuboid specimens (Fig. 5a) reveal the 3D geometry of shock melt veins (Fig. 5b). In the examined samples, cooling-induced contraction cracks are mainly confined within the shock melt veins, and no systematic propagation of these cracks into the surrounding host rock was observed at the SEM and CT observation scales. Cooling-induced contraction cracks appear as polygonal networks perpendicular to vein surfaces (Fig. 5c); viewed parallel to the surface, cracks are preferentially aligned (Fig. 5d), although perpendicular views reveal polygonal, near-hexahedral patterns (Fig. 5e). These veins formed during high-velocity impacts, where shock melting was followed by rapid quenching in space. Solidification generated contraction cracks that propagated inward from vein surfaces under thermal stress, forming polygonal patterns. Such cooling-induced contraction crack networks resemble columnar jointing in terrestrial basalts, where hexagonal cross-sections arise from fracture mechanics (Hofmann et al. 2015).

3.5 Coupling Effects of Mineral Strengthening and Crack Weakening on Rocks

3.5.1 Mechanical Properties of Rocks

As shown in Fig. 6a, the effect of shock melt veins is discussed numerically. We established three different accurate grain-based models (Fig. 6a-1) based on the results of micro-scale experiments. Sim^1 does not contain shock melt vein, Sim^2_{melt} contains shock melt veins without cooling-induced contraction cracks, and Sim^3_{crack} contains shock melt veins with cooling-induced contraction cracks. (Fig. 6c) shows the stress–strain curves obtained from the uniaxial compression simulations, from which the elastic modulus and uniaxial compressive strength were calculated. The elastic modulus and uniaxial compressive strengths of the three samples are shown in Table 1.

As shown in Fig. 6b, to discuss the influence of shock melt veins experimentally, meteorites were processed into cylindrical specimens with a height of 2 cm and a diameter

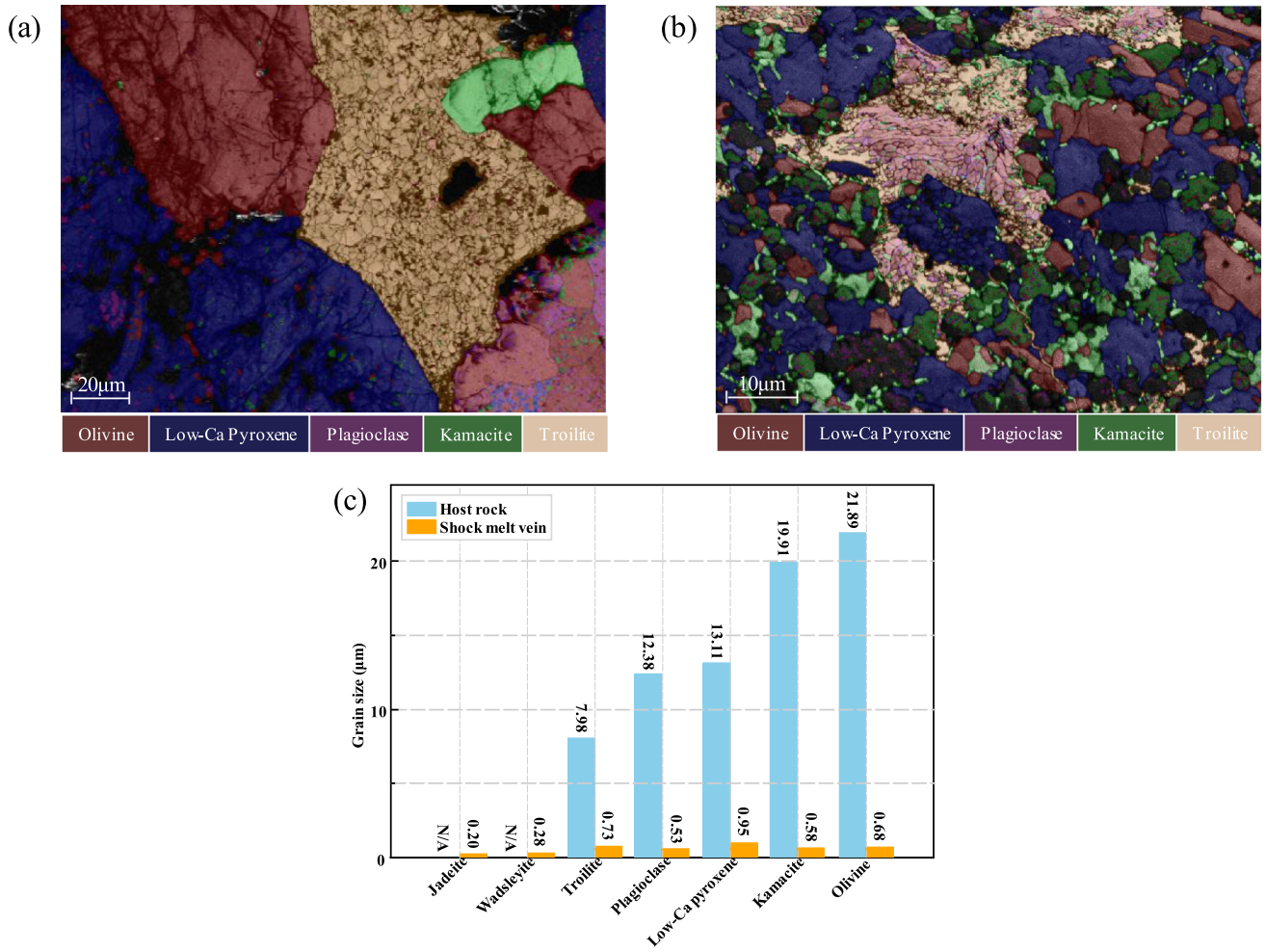

Fig. 3 Shock-induced grain refinement. **a** Minerals in host rock; **b** minerals in shock melt veins; **c** crystal grain size comparison between host rock and shock melt veins

of 1 cm. Among these, samples $Mech^1$, $Mech^2$ and $Mech^3$ contain no shock melt veins, although samples $Mech^4_{melt}$, $Mech^5_{melt}$ and $Mech^6_{melt}$ contain shock melt veins without cooling-induced contraction cracks. Because meteorite specimens with well-developed cooling-induced contraction cracks are scarce and easily damaged during preparation, their compressive response was evaluated only through numerical simulation. The elastic modulus and uniaxial compressive strength, calculated from the stress–strain curves obtained in the uniaxial compression tests (Fig. 6c), are presented in Table 1.

3.5.2 Wave Velocity of Rocks

In this section, the effects of shock melt veins on wave velocity of rocks are discussed experimentally. Four different samples were prepared (Fig. 7a). $Wave^1$ does not contain shock melt vein, $Wave^2_{melt}$ contains a fine shock melt vein without cooling-induced contraction cracks, $Wave^3_{melt}$ contains a coarse shock melt veins without cooling-induced contraction cracks, $Wave^4_{crack}$ contains both coarse shock melt veins and cooling-induced contraction cracks. The results are shown in Table 1.

3.5.3 Comprehensive Analysis for the Physical–Mechanical Properties of Rocks

The results in Table 1 show that shock melt veins without cooling-induced contraction cracks can enhance the mechanical properties and wave velocity of rocks, whereas the presence of cooling-induced contraction cracks significantly weakens the mechanical performance and reduces wave velocity. Samples containing shock melt veins exhibit increases of approximately

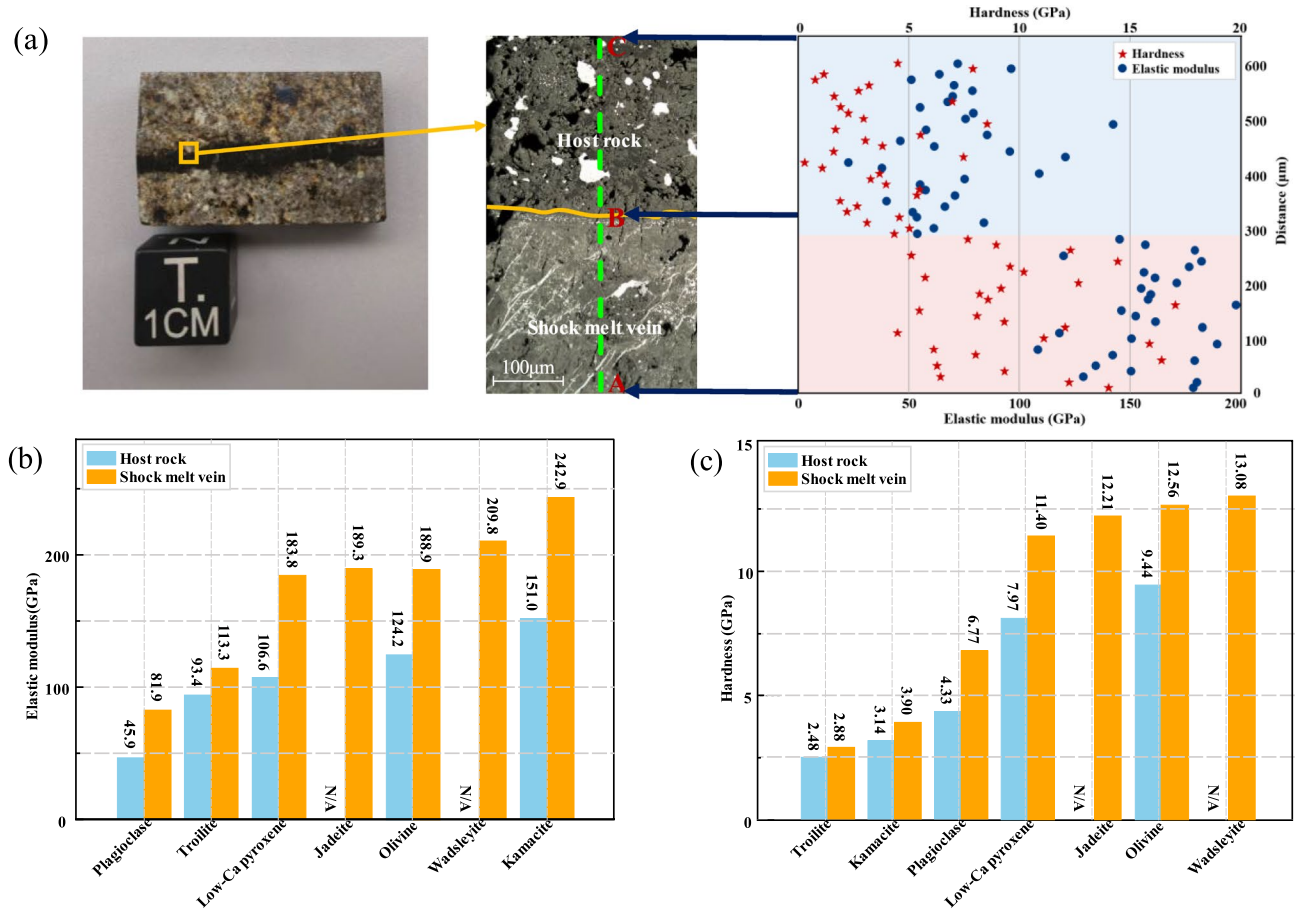

Fig. 4 Shock-induced strengthening of minerals. **a** Elastic modulus distribution; **b** Elastic modulus comparison; **c** hardness comparison between host rock and shock melt veins

20–50% in elastic modulus, uniaxial compressive strength, and P-wave velocity compared with vein-free samples; however, once cooling-induced contraction cracks develop within the shock melt veins, the P-wave velocity drops abruptly by about 50%.

4 Discussion

4.1 Shock-Induced Nanostructuring as a Strengthening Mechanism of Rock-Forming Minerals

Our results demonstrate that high-velocity impacts not only trigger phase transitions, such as the formation of wadsleyite and jadeite, but also refine the crystal grain sizes of both transformed and untransformed minerals to the sub-micrometre scale. This nanoscale restructuring increases resistance to deformation, elevating elastic moduli and hardness across all major mineral phases. Importantly, even minerals that remain crystallographically unaltered exhibit enhanced mechanical properties due to grain refinement, indicating that shock-induced grain refinement itself can act as an effective mineral-scale strengthening mechanism. This finding expands planetary material classification beyond phase symmetry alone, highlighting nanomechanics as a fundamental dimension of impact metamorphism.

4.2 Implications for Physical–Mechanical Properties of Planetary Rocks

Our study establishes a cross-scale "crystal grain-mineral-rock" framework that links shock-induced mineral strengthening to rock behavior, providing a new perspective for interpreting planetary seismic observations. At the rock scale, physical properties reflect a balance between mineral strengthening and crack weakening. Cooling-induced contraction cracks within shock melt veins dominate the mechanical response, reducing mechanical strength and P-wave velocity. In contrast, where cracks are absent, nanoscale restructuring of minerals prevails, enhancing

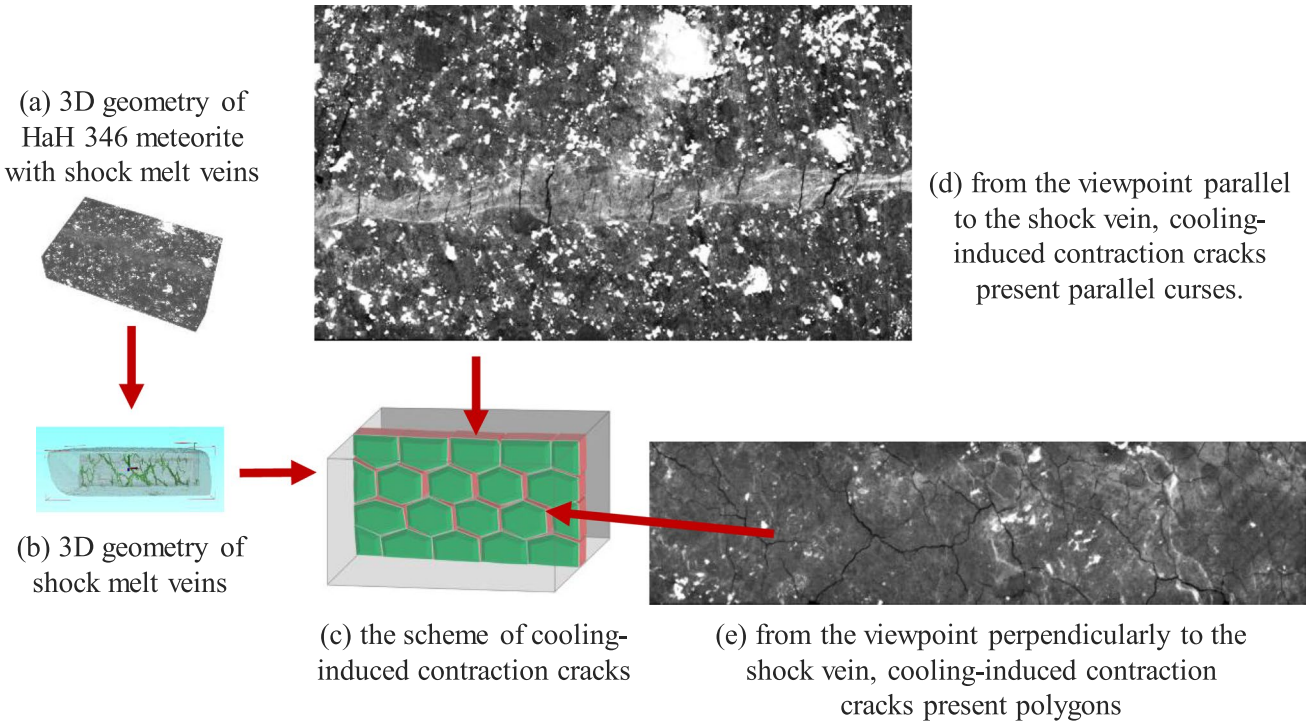

Fig. 5 Cooling-induced contraction cracks in shock melt veins of the HaH346 meteorite

elastic modulus, uniaxial compressive strength, and P-wave velocity by up to 50%. Thus, even within impact structures, regions with sparse fracturing may exhibit mechanical strengthening.

This duality-fracture-induced weakening versus mineral strengthening provides a physical basis for seismic heterogeneity within impact basins. Terrestrial analogues further support this interpretation: laboratory and borehole observations demonstrate that microcracks markedly reduce seismic velocities in metamorphic rocks, while velocity recovers as cracks diminish (Kästner et al. 2020). In the Chesapeake Bay impact structure, porous suevite and impact melt rocks display low velocities, whereas granite blocks with fewer fractures maintain relatively higher velocities (Christeson et al. 2018). Similarly, at Charlevoix, seismic tomography reveals low-velocity zones inside the crater linked to pervasive fracturing and elevated porosity, while unfractured rocks outside the crater retain higher velocities (Onwuemeka et al. 2021).

Extending these observations to airless or weak-atmosphere planetary bodies, such as asteroids and the Moon, this mechanical duality between fracture-induced weakening and mineral strengthening implies that the effective mechanical behavior of impact-processed materials is controlled not only by bulk composition or shock stage, but also by the spatial coupling between strengthening processes (grain refinement, phase transformation, and densification) and damage structures (microcracking, contraction cracking, and porosity development). Such shock-induced heterogeneous architectures, produced by repeated impact processing, are a fundamental characteristic of ordinary chondrite parent bodies (Kohout et al. 2017; Bischoff et al. 2019). Moreover, the recently reported positive correlation between shock stage and petrologic type in ordinary chondrites suggests that impact-induced mechanical modification may be coupled with parent-body thermal metamorphism, because petrologic type generally reflects the degree of thermal metamorphic overprinting (Rubin 2025). These coupled shock-metamorphic heterogeneities likely govern asteroid-scale mechanical behavior, including effective strength, seismic wave attenuation, and catastrophic disruption thresholds (Britt et al. 2002; Richardson et al. 2005; Kohout et al. 2020). By contrast, for planetary bodies with substantial atmospheres or active surface modification, such as Earth and Mars, the original shock-induced mechanical signatures may be partly overprinted by atmospheric filtering of impactors, erosion, aqueous alteration, thermal alteration, and tectonic or sedimentary processes (French and Koeberl 2010; Popova et al. 2003; Schmieder and Kring 2020). Therefore, the framework proposed here is most directly applicable to airless or weak-atmosphere bodies where impact-generated microstructures and damage architectures are more likely to be preserved (Crawford et al. 2021).

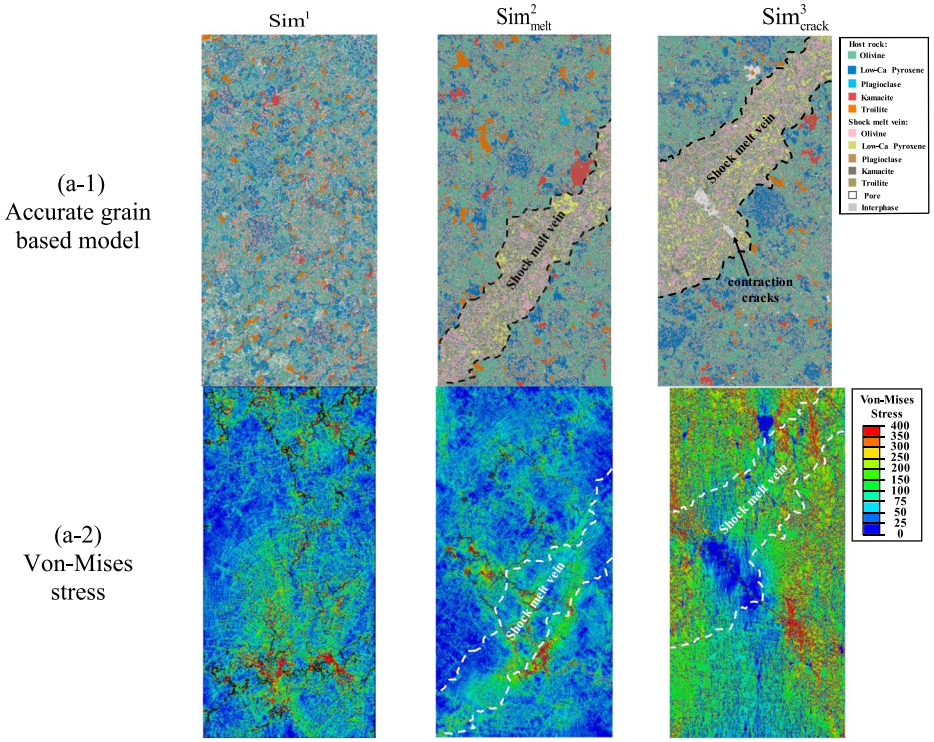

(a) Numerical investigation of the effect of shock melt veins

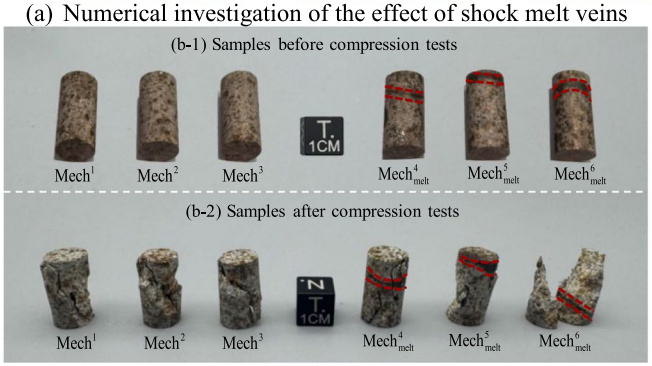

(b) Experimental samples used to investigate the effect of shock melt veins on mechanical property

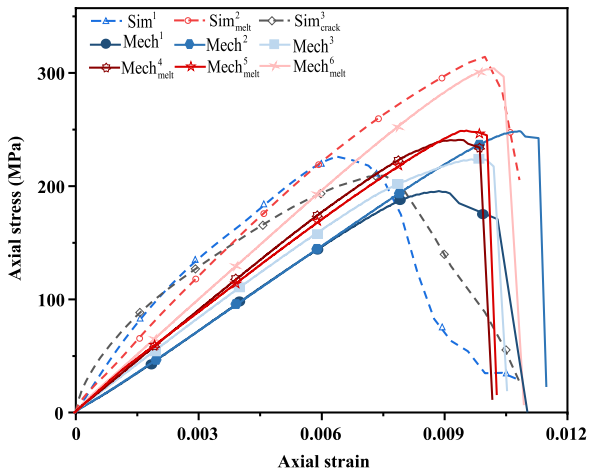

(c) The stress-strain curves of compression testing achieved by numerical modelling and experiments

Fig. 6 Numerical and experimental investigation of the effects of shock melt veins on the mechanical properties of rocks. **A** Numerical investigation of the effect of shock melt veins, **B** Experimental samples used to investigate the effect of shock melt veins on mechanical property, **C** The stress–strain curves of compression testing achieved by numerical modeling and experiments

Table 1 Numerical and experimental results for discussing the effect of shock melt veins

Sample condition	Sample ID	Testing parameters		
		Elastic modulus (GPa)	uniaxial compressive strength (MPa)	P-wave velocity (km/s)
No shock melt vein	Sim^{1}	26.83	231.26	–
	$Mech^{1}$	24.52	195.40	-
	$Mech^{2}$	24.46	248.42	-
	$Mech^{3}$	25.90	223.77	-
	$Wave^{1}$	-	-	3.98
Shock melt vein without cooling-induced contraction crack	Sim^{2}_{melt}	30.01	314.16	-
	$Mech^{4}_{melt}$	28.72	240.69	–
	$Mech^{5}_{melt}$	26.24	249.06	–
	$Mech^{6}_{melt}$	31.12	303.08	–
	$Wave^{2}_{melt}$	–	–	4.41
	$Wave^{3}_{melt}$	–	–	4.81
Shock melt vein with cooling-induced contraction crack	Sim^{3}_{crack}	17.96	209.35	–
	$Wave^{4}_{crack}$	–	–	2.31

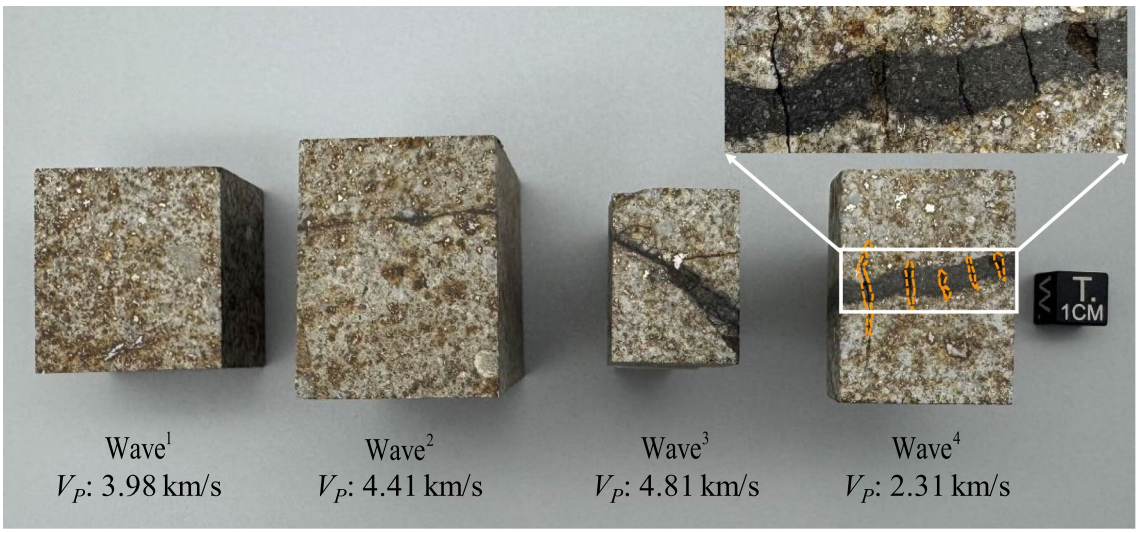

Fig. 7 Experimental samples for discussting the effect of shock melt veins on wave velocity

5 Conclusions

This work establishes a cross-scale framework for investigating the effects of shock melt veins on the crystal-scale, mineral-scale and rock-scale physical–mechanical properties. The main conclusions are as follows:

1. Shock melt veins in HaH 346 ordinary chondrites contain trace high-pressure phases, including wadsleyite and jadeite, which shows pronounced shock-induced grain refinement. The average crystal grain size decreases from 16.71 μm in the host rock to 0.74 μm in the shock melt veins.
2. Nanoindentation results show that minerals within shock melt veins have higher elastic modulus and hardness than the same mineral phases in the host rock. This indicates that shock-induced grain refinement and local phase transformation can enhance the mineral-scale mechanical properties of ordinary chondrites.
3. At rock scale, physical–mechanical properties are governed by the competition between shock-induced mineral strengthening and crack weakening. Where

cooling-induced contraction cracks are absent or limited, mineral-scale strengthening is transferred to the bulk response, increasing elastic modulus, uniaxial compressive strength, and P-wave velocity by approximately 20–50%. However, when contraction cracks develop, crack weakening dominates and P-wave velocity decreases by about 50%, highlighting the competing controls on shocked rock behavior.

Acknowledgements The work was supported by the National Natural Science Foundation of China No.42577189 and No. 12502471.

Author Contributions Yiheng Zhang: Methodology, Investigation, Data Curation, Formal Analysis, Visualization, Writing — Original Draft. Jiangmei Qiao: Methodology, Funding Acquisition. Haifeng Zhao: Visualization. Pengzhi Pan: Visualization. Xuhai Tang: Conceptualization, Investigation, Writing — Review & Editing, Funding Acquisition, Supervision, Resources.

Funding National Natural Science Foundation of China, 42577189, Xuhai Tang, 12502471, Jingmei Qiao

Data Availability Datasets related to this article are made available from a public repository of research data, Mendeley Data, through the following link, https://doi.org/10.17632/fmcyb2txbf.1.

Declarations

Conflict of interest Authors declare that they have no competing interests.

References

Bidgood AK, Parsons AJ, Lloyd GE et al (2021) EBSD-based criteria for coesite-quartz transformation. J Metamorph Geol 39(1):165–180. https://doi.org/10.1111/jmg.12566

Bischoff A, Schleiting M, Patzek M (2019) Shock stage distribution of 2280 ordinary chondrites—Can bulk chondrites with a shock stage of S6 exist as individual rocks? Meteorit Planet Sci 54:2189–2202. https://doi.org/10.1111/maps.13208

Britt DT, Yeomans D, Housen K, Consolmagno G (2002) Asteroid density, porosity, and structure. In: Bottke WF, Cellino A, Paolicchi P, Binzel RP (eds) Asteroids III. University of Arizona Press, Tucson, pp 485–500

Chen M, El Goresy A, Gillet P (2004) Rinawoodite lamellae in olivine: clues to olivine-ringwoodite phase transition mechanisms in shocked meteorites and subducting slabs. Proc Natl Acad Sci U S A 101(42):15033–15037. https://doi.org/10.1073/pnas.0405048101

Christeson GL, Gulick SPS, Morgan JV et al (2018) Extraordinary rocks from the peak ring of the Chicxulub impact crater: P-wave velocity, density, and porosity measurements from IODP/ICDP Expedition 364. Earth Planet Sci Lett 498:1–11. https://doi.org/10.1016/j.epsl.2018.05.013

Collins GS, Melosh HJ, Ivanov BA (2004) Modeling damage and deformation in impact simulations. Meteorit Planet Sci 39(2):217–231. https://doi.org/10.1111/j.1945-5100.2004.tb00337.x

Collins GS, Patel N, Davison TM et al (2020) A steeply-inclined trajectory for the chicxulub impact. Nat Commun. https://doi.org/10.1038/s41467-020-15269-x

Crawford IA, Joy KH, Pasckert JH, Hiesinger H (2021) The lunar surface as a recorder of astrophysical processes. Philos Trans R Soc A Math Phys Eng Sci 379:20190562. https://doi.org/10.1098/rsta.2019.0562

French BM, Koeberl C (2010) The convincing identification of terrestrial meteorite impact structures: what works, what doesn't, and why. Earth-Sci Rev 98:123–170. https://doi.org/10.1016/j.earscirev.2009.10.009

Fritz J, Greshake A (2009) High-pressure phases in an ultramafic rock from Mars. Earth Planet Sci Lett 288(3–4):619–623. https://doi.org/10.1016/j.epsl.2009.10.030

Ghent RR, Carter LM, Bandfield JL et al (2016) Lunar crater ejecta: physical properties revealed by radar and thermal infrared observations. Icarus 273:182–195. https://doi.org/10.1016/j.icarus.2015.12.014

Grebol-Tomas P, Ibanez-Insa J, Trigo-Rodriguez JM et al (2025) Mechanical softening of lunar olivine probed via nanoindentation and high-pressure x-ray diffraction measurements. Geosci Front. https://doi.org/10.1016/j.gsf.2025.102110

Hofmann M, Anderssohn R, Bahr HA et al (2015) Why hexagonal basalt columns? Phys Rev Lett 115(15):154301. https://doi.org/10.1103/PhysRevLett.115.154301

Hrstka T, Gottlieb P, Skála R et al (2018) Automated mineralogy and petrology - applications of tescan integrated mineral analyzer (tima). J Geosci 63(1):47–63

Jaeger JC, Cook NGW, Zimmerman RW (2007) Fundamentals of Rock Mechanics, 4th edn. Wiley-Blackwell, Chichester

Kästner F, Pierdominici S, Elger J et al (2020) Correlation of core and downhole seismic velocities in high-pressure metamorphic rocks: a case study for the COSC-1 borehole. Sweden Solid Earth 11(2):607–626. https://doi.org/10.5194/se-11-607-2020

Khan A, Ceylan S, van Driel M et al (2021) Upper mantle structure of mars from insight seismic data. Sci 373(6553):434–438. https://doi.org/10.1126/science.abf2966

Kohout T, Gritsevich M, Grokhovsky VI, Yakovlev GA, Haloda J, Halodova P, Michallik RM, Penttilä A, Muinonen K (2017) Annama H chondrite—mineralogy, physical properties, cosmic ray exposure, and parent body history. Meteorit Planet Sci 52:1525–1551. https://doi.org/10.1111/maps.12871

Kohout T, Penttilä A, Mann P et al (2020) Distinguishing between shock-darkening and space-weathering trends in ordinary chondrite reflectance spectra. Planet Sci J 1:37. https://doi.org/10.3847/PSJ/aba7c2

Kronyak RE, Arndt C, Kah LC et al (2020) Predicting the Mechanical and Fracture Properties of Mars Analog Sedimentary Lithologies. Earth Space Sci. https://doi.org/10.1029/2019EA000926

Li CL, Su Y, Pettinelli E et al (2020) The Moon's farside shallow subsurface structure unveiled by Chang'E-4 Lunar Penetrating Radar. Sci Adv. https://doi.org/10.1126/sciadv.aay6898

Mangold N, Gupta S, Gasnault O et al (2021) Perseverance rover reveals an ancient delta-lake system and flood deposits at Jezero crater. Mars Sci 374(6568):711–717. https://doi.org/10.1126/science.abl4051

Miyahara M, Ozawa S, Ohtani E et al (2013) Jadeite formation in shocked ordinary chondrites. Earth Planet Sci Lett 373:102–108. https://doi.org/10.1016/j.epsl.2013.04.023

Moyano-Cambero CE, Pellicer E, Trigo-Rodríguez JM et al (2017a) Nanoindenting the chelyabinsk meteorite to learn about impact deflection effects in asteroids. Astrophys J 835:157. https://doi.org/10.3847/1538-4357/835/2/157

Moyano-Cambero CE, Trigo-Rodríguez JM, Pellicer E et al (2017b) Chelyabinsk meteorite as a proxy for studying the properties of potentially hazardous asteroids and impact deflection strategies.

In: Trigo-Rodríguez JM, Gritsevich M, Palme H (eds) Assessment and mitigation of asteroid impact hazards. Astrophysics and Space Science Proceedings 46: 219–241. https://doi.org/10.1007/978-3-319-46179-3_11

Nie JY, Wang SQ, Cui YF et al (2025) Analyzing the mechanical heterogeneity of the chang'e-5 lunar breccia clast: implications for the elastic modulus of lunar rock. J Geophys Res Planets. https://doi.org/10.1029/2024JE008849

Oliver WC, Pharr GM (1992) An improved technique for determining hardness and elastic modulus using load and displacement sensing indentation experiments. J Mater Res 7(6):1564–1583. https://doi.org/10.1557/JMR.1992.1564

Onwuemeka J, Liu Y, Harrington RM (2021) Crustal Velocity Variations and Constraints on Material Properties in the Charlevoix Seismic Zone. J Geophys Res Solid Earth Eastern Canada. https://doi.org/10.1029/2020JB020918

Orosei R, Lauro SE, Pettinelli E et al (2018) Radar evidence of subglacial liquid water on Mars. Sci 361(6401):490–493. https://doi.org/10.1126/science.aar7268

Popova O, Nemtchinov I, Hartmann WK (2003) Bolides in the present and past martian atmosphere and effects on cratering processes. Meteorit Planet Sci 38:905–925. https://doi.org/10.1111/j.1945-5100.2003.tb00287.x

Richardson JE, Melosh HJ, Greenberg R, O'Brien DP (2005) The global effects of impact-induced seismic activity on fractured asteroid surface morphology. Icarus 179:325–349. https://doi.org/10.1016/j.icarus.2005.07.005

Robin CQ, Duchene A, Murdoch N et al (2024) Mechanical properties of rubble pile asteroids (Dimorphos, Itokawa, Ryugu, and Bennu) through surface boulder morphological analysis. Nat Commun. https://doi.org/10.1038/s41467-024-50147-w

Rubin AE (2025) Positive correlation between shock stage and petrologic type in ordinary chondrites: Implications for the internal structures and thermal histories of ordinary-chondrite parent asteroids. Meteorit Planet Sci 60:17–31. https://doi.org/10.1111/maps.14284

Schmieder M, Kring DA (2020) Earth's impact events through geologic time: a list of recommended ages for terrestrial impact structures and deposits. Astrobiology 20:91–141. https://doi.org/10.1089/ast.2019.2085

Spohn T, Grott M, Smrekar SE et al (2018) The heat flow and physical properties package (hp3) for the insight mission. Space Sci Rev. https://doi.org/10.1007/s11214-018-0531-4

Tanbakouei S, Trigo-Rodríguez JM, Sort J et al (2019) Mechanical properties of particles from the surface of asteroid 25143 Itokawa. Astron Astrophys. https://doi.org/10.1051/0004-6361/201935380

Tang X, Zhang Y, Xu J et al (2022) Determining young's modulus of granite using accurate grain-based modeling with microscale rock mechanical experiments. Int J Rock Mech Min Sci 157:105167. https://doi.org/10.1016/j.ijrmms.2022.105167

Tang X, Xu J, Zhang Y et al (2023) The rock-forming minerals and macroscale mechanical properties of asteroid rocks. Eng Geol 321:107154. https://doi.org/10.1016/j.enggeo.2023.107154

Vasavada AR (2022) Mission overview and scientific contributions from the mars science laboratory curiosity rover after eight years of surface operations. Space Sci Rev. https://doi.org/10.1007/s11214-022-00882-7

Witze A (2021) Why NASA's mars rover failed to collect its first rock core. Nature. https://doi.org/10.1038/d41586-021-02208-z

Xiao WB, Carrasco S, Xu ZB et al (2025) Subsurface fluvial sediments beneath insight on mars from geophysical constraints. Commun Earth Environ. https://doi.org/10.1038/s43247-025-02777-1

Xu JJ, Zhang YH, Rutqvist J et al (2023) Thermally induced microcracks in granite and their effect on the macroscale mechanical behavior. J Geophys Res Solid Earth. https://doi.org/10.1029/2022JB024920

Publisher's Note Springer Nature remains neutral with regard to jurisdictional claims in published maps and institutional affiliations.

Springer Nature or its licensor (e.g. a society or other partner) holds exclusive rights to this article under a publishing agreement with the author(s) or other rightsholder(s); author self-archiving of the accepted manuscript version of this article is solely governed by the terms of such publishing agreement and applicable law.